ISSN (Print) 1226-1750
ISSN (Online) 2233-6656
Journal of Magnetics 30(4), 725-732 (2025) https://doi.org/10.4283/JMAG.2025.30.4.725

Dosimetric Impact of Beam Configuration and Tumor Geometry on 3D-Conformal Therapy with Electromagnetic Radiation for Hepatocellular Carcinoma

Jeong Ho Kim*

Dept. of Radiology, Daejeon Health University, Chungjung ro, Republic of Korea

(Received 27 October 2025, Received in final form 25 December 2025, Accepted 26 December 2025)

This phantom study evaluated the impact of tumor geometry and treatment parameters on dose distribution for hepatocellular carcinoma using three-dimensional conformal therapy with electromagnetic radiation. A CT simulation phantom was used to model spherical tumors of varying sizes and locations. We analyzed dosimetric outcomes for plans using 3, 4, and 6 electromagnetic radiation fields, with and without wedge filters. Plan quality significantly deteriorated for large and centrally located tumors, which exhibited poor target coverage and conformity. Conversely, small, peripheral tumors were treated effectively. Wedge filters improved conformity for large tumors but had minimal impact on central tumors. While 3D-CRT is a viable option for small, peripherally located HCC, it has significant limitations for large or central tumors. These findings provide a dosimetric rationale for prioritizing advanced techniques like IMRT or SBRT for these more challenging cases.

Keywords : hepatocellular carcinoma, elecromagnetic radiation Therapy, dosimetric phantom study, 3D-CRT

1. Introduction

The human body is composed of various organs that perform intrinsic physiological functions [1]. Major organs such as the liver, lungs, heart, kidneys, stomach, and intestines act synergistically to maintain life and regulate homeostasis [2]. Among these, the liver is the largest internal organ and mediates diverse physiological roles including detoxification, protein synthesis, coagulation factor production, bile secretion, and regulation of nutrient metabolism [3]. Due to the liver's multi-functionality and anatomical location, malignant tumors arising in the liver can have a critical impact on systemic health [4]. Hepatocellular carcinoma (HCC), in particular, is characterized by late symptom onset and rapid progression, making early diagnosis challenging [5]. The timing and modality of treatment selection critically influence patient survival outcomes [6, 7]. According to the World Health Organization (WHO) and national statistics, liver cancer ranks as the fifth most common malignancy worldwide and is among the leading causes of cancer-related mortality [8, 9]. The prevalence of chronic liver diseases such as hepatitis B virus (HBV), hepatitis C virus (HCV), and cirrhosis is notably high in countries including South Korea, China, and Southeast Asia, contributing to elevated incidence rates of HCC [10, 11]. In South Korea, liver cancer is the second leading cause of cancer-related death in males and ranks fourth in females, predominantly affecting individuals over 50 years of age [12]. Treatment outcomes for HCC vary significantly depending on the tumor stage and therapeutic approach [13]. Early-stage HCC can achieve a 5-year overall survival rate exceeding 70% through interventions such as surgical resection, radiofrequency ablation (RFA), localized electromagnetic radiation therapy, and liver transplantation [14, 15]. However, advanced-stage HCC continues to have a poor prognosis, with 5-year survival rates ranging between 10% and 20% [16]. Therefore, the importance of early detection and precision therapy using electromagnetic radiation in HCC management is increasingly emphasized [17]. Treatment planning must prioritize liver function preservation alongside high-precision targeted therapy to the tumor [18,19]. Moreover, therapeutic decisions are influenced by patient-specific factors including hepatic functional reserve, tumor location and size, and disease stage [20]. Historically, therapy using electromagnetic radiation for liver tumors was limited due to the radiosensitivity of

*Corresponding author: Tel: +82-42-670-9176
Fax: +82-42-670-9564, e-mail: map@hit.ac.kr

hepatic parenchyma [21, 22]. However, advancements in high-precision techniques using electromagnetic radiation now allow selective delivery of high doses of electromagnetic radiation to tumors while sparing normal liver tissue [23]. Contemporary modalities for therapy with electromagnetic radiation for HCC, such as intensity-modulated electromagnetic radiation therapy (IMRT), stereotactic body electromagnetic radiation therapy (SBRT), image-guided electromagnetic radiation therapy (IGRT), and four-dimensional electromagnetic radiation therapy (4D RT), have been rapidly adopted [24]. Nonetheless, due to economic, personnel, and technical constraints, three-dimensional conformal electromagnetic radiation therapy (3D-CRT) remains widely utilized [25, 26]. In complex anatomical regions like the liver, where normal tissues including the gastrointestinal tract and kidneys surround the tumor, three-dimensional dose distribution analysis is a critical determinant of treatment plan efficacy and safety [27]. Hence, formulating treatment planning guidelines is essential [28]. Given the liver's large volume and morphological variability, it is necessary to evaluate dose distributions by varying tumor location and size [29]. This study aims to assess dose distributions according to the number of electromagnetic radiation fields and wedge filter angles based on tumor location and size in HCC. The findings will provide appropriate criteria for treatment planning and serve as foundational data for the standardization and comparative evaluation of advanced precision techniques using electromagnetic radiation such as IMRT and SBRT in the future.

2. Materials and Methods

2.1. Study Subjects

This study was conducted using a CT simulation phantom, not a clinical study involving human subjects. The virtual hepatocellular carcinoma tumor was modeled according to the following criteria.

(1) Tumor Location: Posteroinferior segment of the right hepatic lobe, central right hepatic lobe, and antero-medial segment of the right hepatic lobe

(2) Tumor Shape: Spherical with diameters of 5 mm, 10 mm, and 20 mm, respectively

(3) Normal Organs at Risk: Liver parenchyma, right lung, left lung, heart, spinal cord, esophagus, stomach, spleen, right kidney, and left kidney

2.2. Methodology

(1) Irradiation Conditions

Beam directions were applied according to the number of fields listed in Table 1, with detailed simulation setups for 3, 4, and 6-portal plans illustrated in Figs. 1, 2, and 3, respectively. Detailed conditions were applied as per

Table 1. Composition of irradiation direction by number of portals.

# of portal	Application directions
3 portals	AP, LAO, RAO
4 portals	AP, LAO, RAO, PA
6 portals	AP, LAO, RAO, PA, LPO, RPO

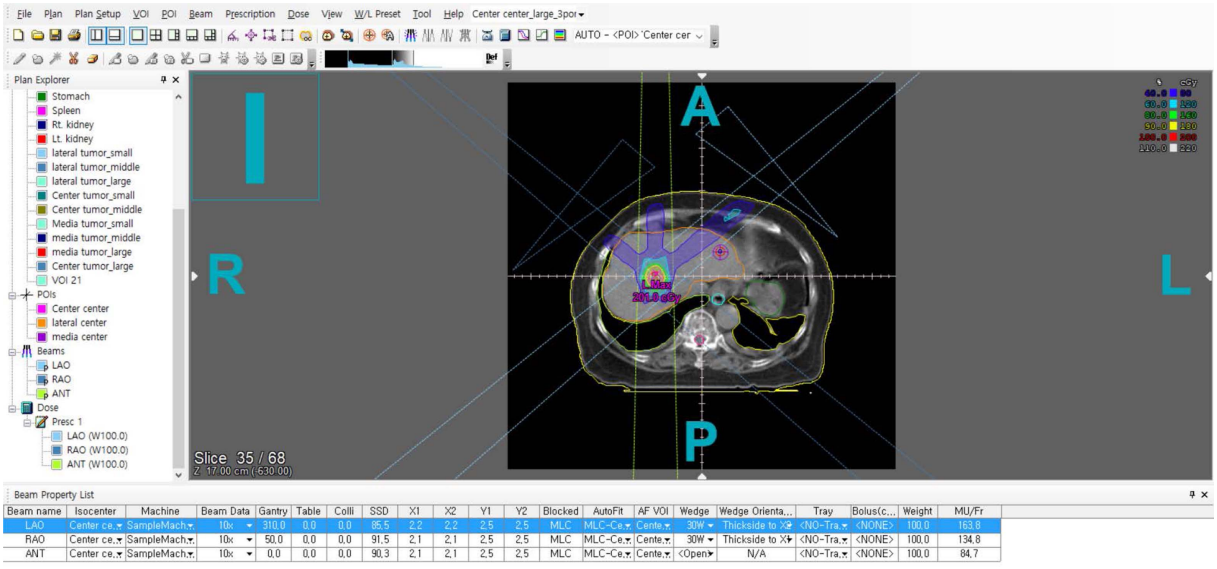

Fig. 1. (Color online) 3-portal treatment plan for HCC tumors using a core plan.

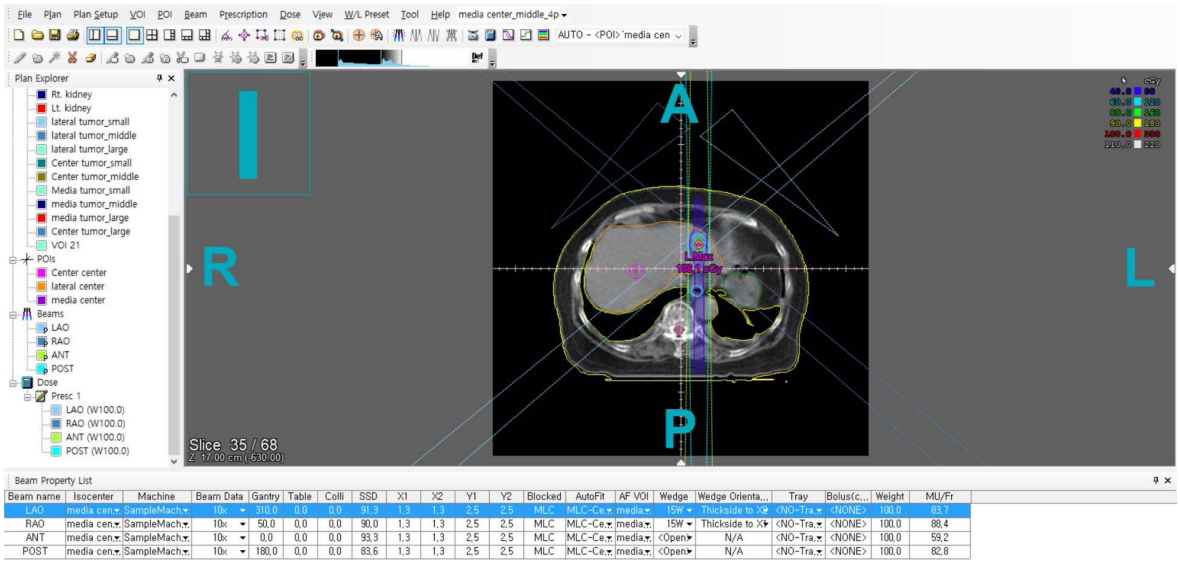

Fig. 2. (Color online) 4-portal treatment plan for HCC tumors using a core plan.

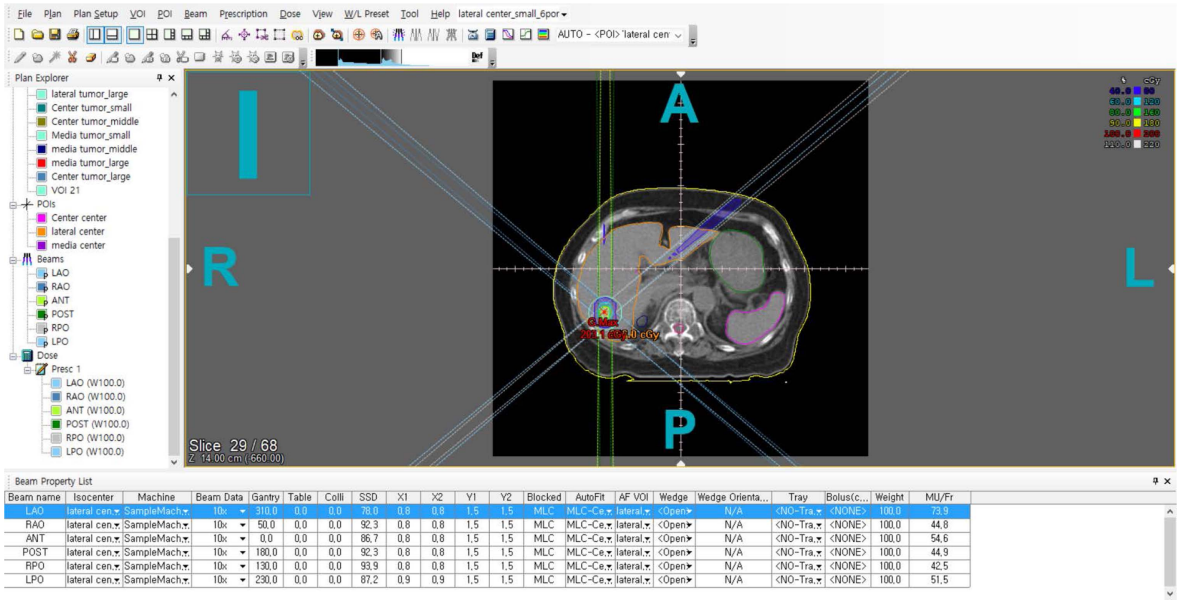

Fig. 3. (Color online) 6-portal treatment plan for HCC tumors using a core plan.

Table 2. Application conditions and wedge filter angle by irradiation direction.

Beam Direction	Radiation Type	Radiation Energy	Gantry Angle	Collimator Angle	Field Size	Wedge Filter
AP	Photon	10 MV	0°	0°	Auto FOV	Not applicable
LAO	Photon	10 MV	50°	0°	Auto FOV	In some cases
RAO	Photon	10 MV	310°	0°	Auto FOV	In some cases
PA	Photon	10 MV	180°	0°	Auto FOV	Not applicable
LPO	Photon	10 MV	140°	0°	Auto FOV	Not applicable
RPO	Photon	10 MV	220°	0°	Auto FOV	Not applicable

Table 2, and the prescribed dose was set at 200 cGy per fraction to the tumor isocenter. The 6-field irradiation setup (Fig. 3) was specifically applied to establish a comparative baseline for IMRT. In the cases of 3-field and 4-field irradiation, wedge filters were applied only to the left anterior oblique (LAO) and right anterior oblique (RAO) fields, with wedge angles categorized as 15°, 30°, 45°, and 60°. The wedge directions were set to face each other with the smallest internal angle, and the thickness was set to be close. The PTV (Planning Target Volume) was provided with a 5 mm margin from the CTV (Clinical Target Volume).

(2) Treatment Planning Simulation and Analysis

Treatment planning was performed using the Core-plan electromagnetic radiation therapy planning system (C&J, Korea), applying the Pencil Beam Convolution (PBC) dose calculation algorithm. Analysis of the treatment plan simulation results included D95%(dose covering 95% of the target volume), Dmean (mean dose), CI (Conformity Index), and HI (Homogeneity Index) for tumor dose assessment, and (maximum dose), V20 (volume receiving ≥20 Gy), and V30 (volume receiving ≥30 Gy) for normal organ dose assessment. All simulation results were quantitatively analyzed in accordance with the guidelines of the American Society for Electromagnetic Radiation Oncology (ASTRO) and the ICRU Report 83.

3. Results

3.1. Results According to Number of Beams

The outcomes for different tumor locations according to the number of electromagnetic radiation beams are summarized in Table 1, Fig. 4, Fig. 5, and the results for various tumor sizes are presented in Table 2, Fig. 6, Fig. 7. D95% ranged from 175.56 cGy to 193.69 cGy, and Dmean from 193.23 cGy to 199.73 cGy. CI values ranged from 29.03 to 65.32, and HI from 0.06 to 0.17. For organs at risk, Dmax(maximum dose) ranged from 35.5 cGy to 70.21 cGy; V20 and V30 ranged from 2.45–7.18 cc and 2.05–6.02 cc, respectively.

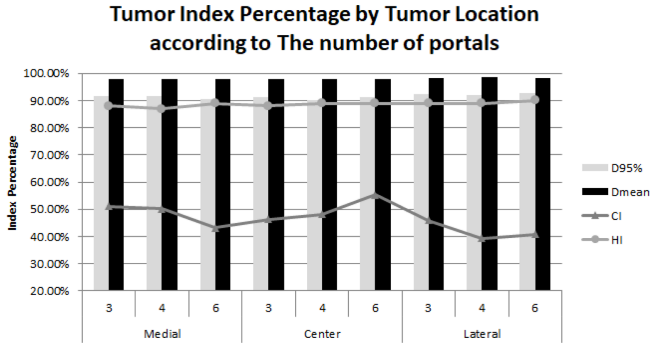

Fig. 4. Tumor index by tumor location according to the number of portals.

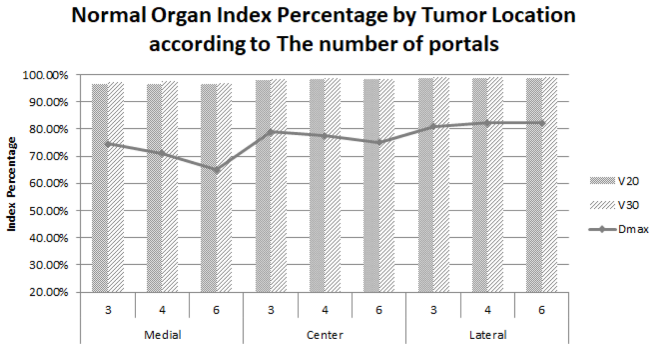

Fig. 5. Normal organ index by tumor location according to the number of portals.

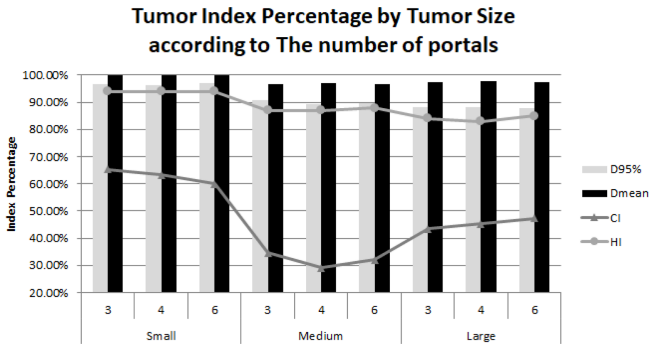

Fig. 6. Tumor index by tumor size according to the number of portals.

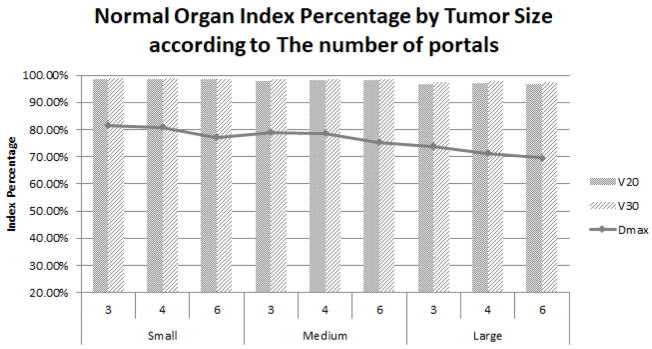

Fig. 7. Normal organ index by tumor size according to the number of portals.

3.2. Results According to Wedge Filter Angle

The dosimetric outcomes for different tumor locations based on the wedge filter angle are presented in Table 5 (as well as Table 3) and Figs. 8, 9. Furthermore, the results for various tumor sizes according to the wedge

Table 3. Tumor and normal organ index results by tumor location according to number of portals.

# of portal	Tumor Location	Tumor Index				Normal Organ Index		
		D95%[1)]	Dmean[1)]	CI	HI	Dmax[1)]	V20[2)]	V30[2)]
3 Portal	Medial	183.59	195.64	51.11	0.12	50.89	7.18	5.67
	Center	182.29	195.88	46.32	0.12	42.17	3.73	3.11
	Lateral	184.87	196.30	45.91	0.11	38.06	2.51	2.18
4 Portal	Medial	183.02	196.03	50.15	0.13	57.99	6.78	4.56
	Center	180.31	195.57	48.10	0.11	45.15	3.44	2.69
	Lateral	184.02	196.99	39.36	0.11	35.50	2.45	2.05
6 Portal	Medial	181.07	195.77	43.25	0.11	70.21	7.03	6.02
	Center	182.35	195.83	55.33	0.11	50.01	3.53	2.99
	Lateral	185.39	196.23	40.83	0.10	35.65	2.49	2.14

1) Unit:[cGy] 2) Unit:[cc]

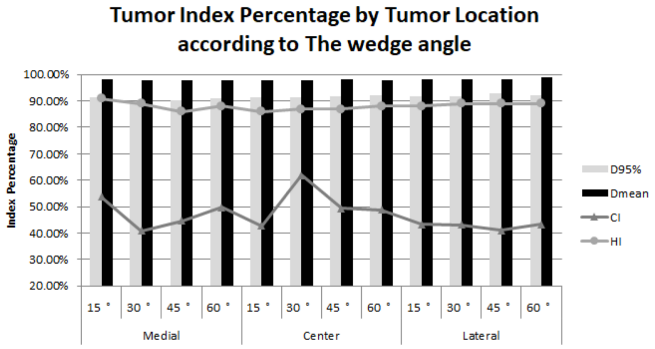

Fig. 8. Tumor index by tumor location according to the wedge angle.

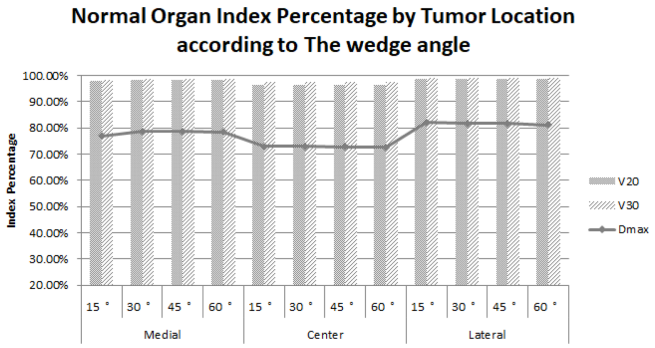

Fig. 9. Normal organ index by tumor location according to the wedge angle.

Table 4. Tumor and normal organ index results by tumor size according to number of portals.

# of portal	Tumor Size	Tumor Index				Normal Organ Index		
		D95%[1)]	Dmean[1)]	CI	HI	Dmax[1)]	V20[2)]	V30[2)]
3 Portal	Small	193.20	199.73	65.32	0.06	36.77	2.95	2.44
	Medium	181.31	193.56	34.65	0.13	42.15	4.13	3.15
	Large	176.24	194.53	43.37	0.16	52.20	6.34	5.37
4 Portal	Small	192.52	199.56	63.28	0.06	38.38	2.75	2.08
	Medium	178.33	193.76	29.03	0.13	42.61	3.74	2.75
	Large	176.50	195.27	45.30	0.17	57.64	6.19	4.48
6 Portal	Small	193.69	199.67	60.00	0.06	45.67	2.93	2.56
	Medium	179.56	193.23	32.12	0.12	49.54	3.88	3.17
	Large	175.56	194.93	47.28	0.15	60.66	6.24	5.42

1) Unit:[cGy] 2) Unit:[cc]

angle are summarized in Table 6 (supplementing Table 4) and Figs. 10, 11. The D95% ranged from 174.77 cGy to 193.36 cGy, and the Dmean ranged from 193.05 cGy to 200.00 cGy. The CI values ranged from 29.56 to 68.21, and the HI ranged from 0.05 to 0.17. For the organs at risk, the Dmax ranged from 36.05 cGy to 55.51 cGy. The V20 and V30 ranged from 2.47 to 7.13 cc and from 2.11 to 5.29 cc, respectively.

Table 5. Tumor and normal organ index results by tumor location according to angle of wedge filter.

Wedge angle	Tumor Location	Tumor Index				Normal Organ Index		
		D95%[1)]	Dmean[1)]	CI	HI	Dmax[1)]	V20[2)]	V30[2)]
15°	Medial	182.91	196.37	53.66	0.09	46.00	3.86	3.08
	Center	182.79	195.62	42.68	0.14	54.20	7.13	5.29
	Lateral	183.66	196.22	43.27	0.12	36.05	2.49	2.13
30°	Medial	179.80	195.77	40.78	0.11	42.76	3.48	2.81
	Center	182.68	195.57	61.82	0.13	54.22	6.89	4.83
	Lateral	183.75	196.30	43.09	0.11	36.46	2.48	2.12
45°	Medial	180.68	195.32	44.62	0.14	42.77	3.48	2.84
	Center	183.40	196.67	49.30	0.13	54.43	6.95	5.15
	Lateral	185.89	196.35	40.96	0.11	36.81	2.48	2.11
60°	Medial	181.78	195.45	49.78	0.12	43.11	3.51	2.88
	Center	184.35	195.48	48.73	0.12	54.91	6.96	5.19
	Lateral	184.49	197.72	43.22	0.11	37.79	2.47	2.11

1) Unit:[cGy] 2) Unit:[cc]

Table 6. Tumor and normal organ index results by tumor size according to angle of wedge filter.

Wedge angle	Tumor Size	Tumor Index				Normal Organ Index		
		D95%[1)]	Dmean[1)]	CI	HI	Dmax[1)]	V20[2)]	V30[2)]
15°	Small	192.45	199.50	63.99	0.06	37.31	2.86	2.26
	Medium	182.14	194.15	36.73	0.12	44.50	4.21	3.15
	Large	174.77	194.55	38.88	0.17	54.44	6.41	5.09
30°	Small	192.60	200.00	63.94	0.05	37.32	2.84	2.25
	Medium	178.69	193.05	31.41	0.13	41.34	3.84	2.87
	Large	174.94	194.58	50.33	0.16	54.79	6.17	4.64
45°	Small	193.03	199.52	68.21	0.07	37.52	2.84	2.25
	Medium	178.85	193.07	29.56	0.13	41.54	3.84	2.89
	Large	178.10	195.75	37.10	0.17	54.96	6.22	4.96
60°	Small	193.36	199.57	61.04	0.06	38.16	2.84	2.28
	Medium	179.60	194.37	29.67	0.12	42.14	3.84	2.89
	Large	177.67	194.72	51.02	0.16	55.51	6.25	5.00

1) Unit:[cGy] 2) Unit:[cc]

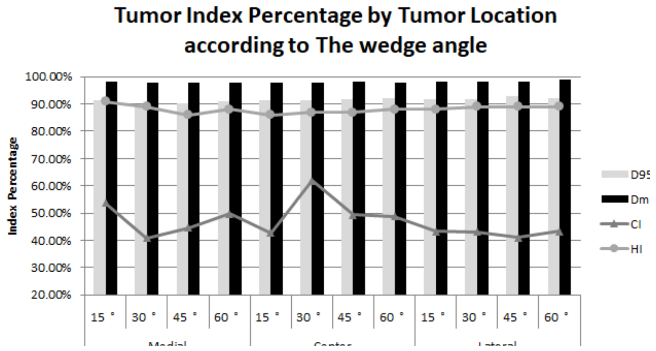

Fig. 10. Tumor index by tumor size according to the wedge angles.

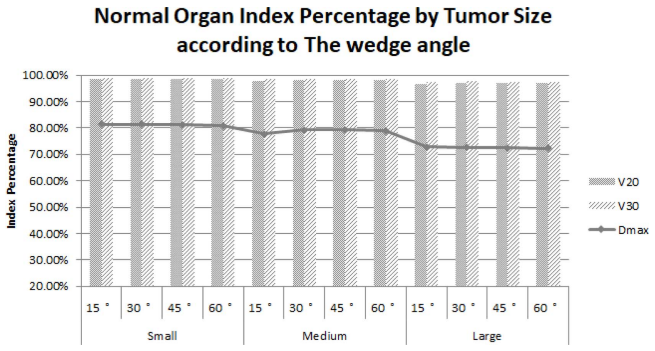

Fig. 11. Normal organ index by tumor size according to the wedge angle.

4. Discussions

This dosimetric phantom study quantitatively analyzed the impact of tumor geometry on dose distribution in 3D-conformal electromagnetic radiation therapy for hepatocellular carcinoma, defining the technique's performance envelope and limitations. The core finding is that 3D-CRT's therapeutic window is heavily dependent on tumor geometry, demonstrating distinct limitations for large or centrally located tumors in delivering adequate target dosage while sparing surrounding organs. This result provides a strong dosimetric rationale for preferentially selecting advanced precision techniques using electromagnetic radiation, such as IMRT or SBRT, when available. Nevertheless, where 3D-CRT remains a necessary tool, these findings serve as a practical guideline: simple field arrangements may suffice for small, lateral tumors, while a strategic approach using wedge filters or combination (e.g., additional fields or advanced techniques) therapy is advisable for larger or central tumors. This study is distinguished by its use of a standardized phantom, isolating the intrinsic performance of the electromagnetic radiation therapy technique from patient-specific anatomical variations. However, this is also its primary limitation, as the static, homogeneous phantom fails to reflect clinical complexities like respiratory motion and tissue heterogeneity. We recognize that precise results are limited, particularly when the number of portals and the tumor size and location are highly constrained. However, the purpose of this study was to provide a more appropriate guideline for the application of 3D-CRT to HCC, not to establish absolute standards, but to limit unnecessary attempts at treatment planning. Therefore, further research is needed to address these limitations and provide more precise guidance. Furthermore, tumor sizes were spaced relatively widely, as smaller tumors are generally more suitable for SBRT. Consequently, tumor sizes were spaced from small to large. As such, the results should be interpreted as a "best-case scenario." Future research should involve studies with real patient data and dynamic phantoms to translate these foundational findings into more clinically significant conclusions.

5. Conclusions

In summary, 3D-CRT is suitable for small peripheral HCC tumors but is suboptimal for large or central tumors due to dose coverage limitations. This study's dosimetric evidence supports using advanced techniques (IMRT, SBRT) for challenging cases, and provides guidance for optimizing 3D-CRT plans when such techniques are not available.

References

[1] G. Billman, Frontiers in Physiology **11**, 1 (2020).
[2] M. E. Kotas and R. Medzhitov, Cell **160**, 816 (2015).
[3] L. Rui, Comprehensive Physiology **4**, 177 (2014).
[4] A. Villanueva, The New England Journal of Medicine **380**, 1450 (2019).
[5] J. M. Llovet, R. K. Kelley, A. Villanueva, A. G. Singal, E. Pikarsky, S. Roayaie, R. Lencioni, K. Koike, J. Zucman-Rossi, and R. S. Finn, Nature Reviews Disease Primers **7**, 6 (2021).
[6] R. Cabrera and D. R. Nelson, Alimentary Pharmacology and Therapeutics **31**, 461 (2010).
[7] M. Kudo, R. S. Finn, S. Qin, K. H. Han, K. Ikeda, F. Piscaglia, A. Baron, J. W. Park, G. Han, J. Jassem, J. F. Blanc, A. Vogel, D. Komov, T. R. J. Evans, C. Lopez, C. Dutcus, M. Guo, K. Saito, S. Kraljevic, T. Tamai, M. Ren, and A. L. Cheng, The Lancet **391**, 1163 (2018).
[8] H. Sung, J. Ferlay, R. L. Siegel, M. Laversanne, I. Soerjomataram, A. Jemal, and F. Bray, A Cancer Journal for Clinicians **71**, 209 (2021).
[9] M. Lawler, L. Murphy, R. Adams, A. L. Agostina, T. Albreht, O. Alatise, A. Barton-Sweeny, P. Borras, J. M. Borras, C. Canbay, P. G. Casali, and P. Croft, The Lancet Oncology **24**, 11 (2023).
[10] J. H. Kao and D. S. Chen, The Lancet Infectious Diseases **2**, 395 (2002).
[11] M. F. Yuen, D. S. Chen, G. M. Dusheiko, H. L. A. Janssen, D. T. Y. Lau, S. A. Locarnini, M. G. Peters, and C. L. Lai, Nature Reviews Disease Primers **4**, 18035 (2018).
[12] M. J. Kang, Y. J. Won, J. J. Lee, K. W. Jung, H. J. Kim, H. J. Kong, J. S. Im, and H. G. Seo, Cancer Research and Treatment **55**, 385 (2023).
[13] M. Reig, A. Forner, J. Rimola, J. Ferrer-Fàbrega, M. Burrel, Á. Garcia-Criado, R. K. Kelley, P. R. Galle, V. Mazzaferro, R. Salem, B. Sangro, A. G. Singal, A. Vogel, J. Fuster, C. Ayuso, and J. Bruix, Journal of Hepatology **76**, 681 (2022).
[14] M. Kudo, Y. Kawamura, K. Hasegawa, R. Tateishi, K. Kariyama, S. Shiina, H. Toyoda, Y. Imai, A. Hiraoka, M. Ikeda, N. Izumi, M. Moriguchi, S. Ogasawara, Y. Minami, K. Ueshima, T. Murakami, S. Miyayama, O. Nakashima, H. Yano, M. Sakamoto, E. Hatano, M. Shimada, N. Kokudo, S. Mochida, and T. Takehara, Liver Cancer, **10**, 181 (2021).
[15] H. El-Serag, Gastroenterology **142**, 1264 (2012).
[16] V. Mazzaferro, E. Regalia, R. Doci, S. Andreola, A. Pulvirenti, F. Bozzetti, F. Montalto, M. Ammatuna, A. Morabito, and L. Gennari, The New England Journal of Medicine **334**, 693 (1996).
[17] J. H. Kim, M. C. Jeon, S. H. Kim, J. S. Kim, and J. W.

Kim, Journal of Magnetics **29**, 518 (2024).
[18] L. A. Dawson, D. Normolle, J. M. Balter, C. J. McGinn, T. S. Lawrence, and R. K. Ten Haken, Int. J. Radiat. Oncol. Biol. Phys. **53**, 810 (2002).
[19] J. E. Kim and Y. M. Jung, Exp. Mol. Med. **49**, 359 (2017).
[20] C.-H. Lo, J.-F. Yang, M.-Y. Liu, Y.-M. Jen, C.-S. Lin, H.-L. Chao, and W.-Y. Huang, PloS one **12**, 0177793 (2017).
[21] B. Emami, J. Lyman, A. Brown, L. Coia, M. Goitein, J. E. Munzenrider, B. Shank, L. J. Wright, and B. Pellett, Int. J. Radiat. Oncol. Biol. Phys. **21**, 109 (1991).
[22] M. A. Hawkins and L. A. Dawson, Cancer **106**, 1653 (2006).
[23] W. S. Ahn, W. Choi, Y. R. Ka, J. Kwak, I.-H. Jung, S. Ahn, and S. S. Shin, Journal of Magnetics **25**, 409 (2020).
[24] S. Apisarnthanarax, A. Barry, M. Cao, B. Czito, R. DeMatteo, M. Drinane, C. L. Hallemeier, E. J. Koay, F. Lasley, J. Meyer, D. Owen, J. Pursley, S. K. Schaub, G. Smith, N. K. Venepalli, G. Zibari, and H. Cardenes, Practical Radiation Oncology **12**, 28 (2022).
[25] S. H. Bae, S. H. Bae, H. C. Park, W. S. Yoon, S. M. Yoon, I.-H. Jung, I. J. Lee, J. W. Kim, J. Seong, T. H. Kim, T.-K. Nam, Y. Choi, S. Y. Lee, H. S. Jang, D. S. Lee, and J. H. Kim, Cancer Res. Treat. **51**, 1589 (2019).
[26] D. H. Wu, L. Liu, and L. H. Chen, World J. Gastroenterol **10**, 2184 (2004).
[27] J.-U. Jang, M.-S. Han, K.-H. Kim, M.-C. Jeon, and U.-J. Hwang, Journal of Magnetics **27**, 430 (2022).
[28] K. E. Poruk, R. Shah, M. S. Grandhi, G. P. Wright, and A. A. Parikh, Annals of Surgical Oncology **30**, 4556 (2023).
[29] Y. Huang, S.-W. Chen, C.-C. Fan, L.-L. Ting, C.-C. Kuo, and J.-F. Chiou, Rakdiaton Oncology **11**, 89 (2016).